Proceedings of
10th European Conference on Turbomachinery Fluid dynamics & Thermodynamics
ETC10, April 15-19, 2013, Lappeenranta, Finland

Numerical simulation of a compressor facility test rig at near-surge operating conditions

F. Crevel [*] *– N. Gourdain* [†] *– F. Wlassow* [‡]

[*]Snecma Villaroche
Rond Point René Ravaud - Réau, 77550 Moissy-Cramayel, France
flore.crevel@cerfacs.fr

[†] CERFACS, Applied Aerodynamics and Multiphysics Team
42 avenue Coriolis, 31057 Toulouse Cedex, France.
nicolas.gourdain@cerfacs.fr.

[‡] Turbomeca
Avenue Joseph Szydlowski, 64511, Bordes, France.
fabien.wlassow@turbomeca.fr

ABSTRACT

Two numerical simulations on the 3.5 stage research compressor CREATE at near-surge conditions have been carried out. The domain of the first simulation consists of the 3.5 stages of the compressor, and this of the second simulation includes the compressor and the complete test rig. The numerical results are first presented and a modal analysis shows that rotating stall occurs in the first simulation, whereas modified surge is found in the second simulation. The analysis of numerical pressure probes located in the compressor and in the test rig allows to assess how the test rig influences the flow and the pressure field. Finally, an acoustic study of the domain is done to explain the differences found between the two configurations.

NOMENCLATURE

f	frequency (Hz)	BPF	Blade Passing Frequency
k	Throttle parameter	CFD	Computational Fluid Dynamics
N_{R_i}	Number of blades of R_i	FFT	Fast Fourier Transform
P_s	Static pressure	(U)RANS	(Unsteady) Reynolds Averaged Navier Stokes
Q	massflow (kg/s)	RSI	Rotor Stator Interaction
Q_n	nominal massflow (kg/s)	STFT	Short Time Fourier Transform
R_i	Rotor number i	λ	wavelength (m)
RSI	Rotor - Stator Interaction	Ω	rotation speed (rad/s)
S_i	Stator number i		

INTRODUCTION

Aerodynamic instabilities in compressors which occur at low massflow, such as stall and surge, need an accurate prediction in order to gain surge margin and thus efficiency. This remains a challenging task in the design process. The compressor operability is greatly influenced by rotor tip clearance dimensions (Inoue et al. (2004)), as the flow in that region often exhibits the first signs of instabilities (Crook et al. (1993); Hoying (1996)). In a multistage configuration, the tip leakage flow of the rotor creates a low axial momentum region which interacts with the downstream stator wake, which then interacts with the following rotor tip leakage flow. As compressors tend to compact, the axial distance between rotors and stators shortens ; therefore the influence of the Rotor Stator Interaction (RSI) and

the unsteadiness of the flow are increased (Callot (2002)). This points out the importance of a better understanding of the dynamics of instabilities.

In this study, rotating stall is first simulated in a 3.5 stage isolated compressor, and the natural periodicity of the compressor is used to reduce the domain to $2\pi/8$. This simulation is then compared to the simulation of the same compressor and its whole test rig, in order to assess the impact of the upstream and downstream volumes of the test rig on the flow. In the past, Greitzer (1976) has shown that downstream volumes promote instabilities with lower frequencies through his B-parameter. That result was confirmed by Spakovszky (2001), who has shown the role of the entire system on the selection of the most unstable frequency, by the analytical models of Tauveron et al. (2006) and by the numerical results of Gourdain et al. (2010).

The rotating instabilities that develop in a compressor have lower frequencies than the phenomena that occur at normal operating conditions in the compressor (Vahdati et al. (2008), Gourdain et al. (2005)), such as the Blade Passing Frequency (BPF). Therefore a simulation of rotating stall requires a simulation on a longer lapse of physical time.

Assumptions such as mixing planes, steady or single blade passages calculations are often used to reduce the cost of the simulation, however they do not allow to simulate rotating stall nor surge properly. With today's high performance computing means, CFD can be used to perform an unsteady simulation of low frequency instabilities on large domains. First, the experimental test case is described, and the numerical methodology is presented, including the meshing strategy and the boundary conditions. Then the theoretical tools used to analyze the results are described. In the last section, the results of both simulations are presented and compared. A computation of the resonant modes of the configuration is proposed to explain the differences between the two simulations.

DESCRIPTION OF THE TEST CASE CREATE

The test rig and the compressor CREATE (Compresseur de Recherche pour l'Etude des effets Aerodynamiques et Technologiques) are studied at Ecole Centrale de Lyon in LMFA (Laboratoire de Mecanique des Fluides et d'Acoustique), France (Ottavy et al. (2012)). The test rig was installed in the early 2000s (Arnaud (2003)). The facility is designed as an open loop and is made of a settling chamber, an air filter and a throttle which drops the pressure to 0.74 of the atmospheric pressure at the inlet of the compressor. After the settling chamber come the upstream strut, the compressor, the downstream strut and the exit. The exit has a throttling butterfly-type valve, just downstream the anti-surge valve, which can quickly discharge the compressor in case of surge. The annular part of the test rig, from the settling chamber to the downstream strut, is axisymetric and has a periodicity of $2\pi/8$ (45°). The exit is fully 3D (Fig.1 (a)).

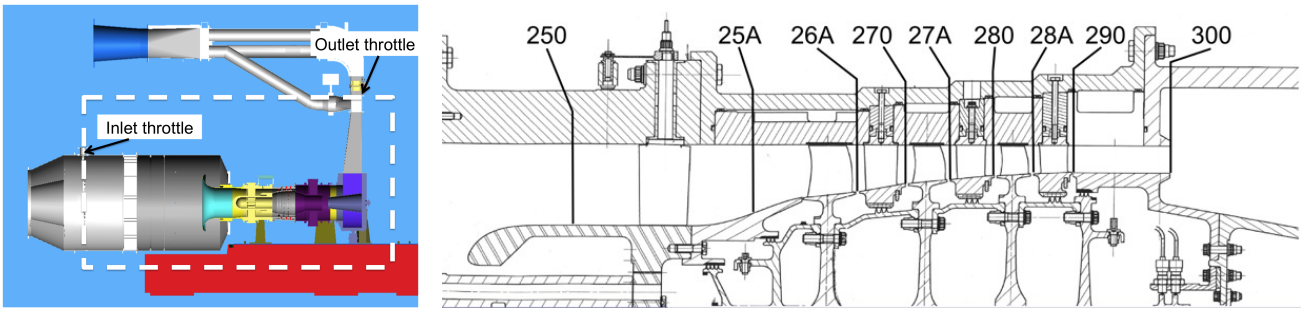

(a) Compressor CREATE test rig

(b) Meridian view of the compressor CREATE

Figure 1: Experimental core compressor CREATE

CREATE is a 3.5-stage research compressor representative of median-rear blocks of modern tur-

bojet engines. It was designed and built by Snecma. The compressor has a spatial periodicity of $2\pi/16$ (see Table 1). In this study, the periodicity of the annular part of the test rig is taken into account, thus the global periodicity of the compressor and test rig is $2\pi/8$. The cylindrical outer casing diameter is 0.52 m and the rotor shaft is driven at the design speed of 11,543 rpm by a 2 MW direct-current drive coupled with a gearbox. The first rotor speed is 313 m.s^{-1} at the tip and the corresponding Mach number is 0.92. The flow is slightly transonic in the first stage and subsonic in the two other ones. In CREATE, the BPF has a frequency of the order of 10^4Hz, rotating stall frequency is of the order of 10^3Hz and the surge frequency is of the order of 1 to 10^2Hz. Therefore rotating stall potentially needs to be simulated on a physical time 10 times longer than a simulation at a nominal operating point, and a surge cycle may require a simulation up to 10^4 times longer to be captured entirely.

Table 1: Blade numbers of the compressor rows

Row	Upstream strut	IGV	R1	S1	R2	S2	R3	S3	Downstream strut
Number of blades (2π)	8	32	64	96	80	112	80	128	8
Number of blades ($2\pi/8$)	1	4	8	12	10	14	10	16	1

NUMERICAL SIMULATIONS

Flow solver and numerical parameters

Rotating stall requires a time accurate method to be correctly captured, therefore it is simulated by solving the Unsteady Reynolds Averaged Navier Stokes (URANS) equations which describe the conservation of mass, momentum and energy of a viscous fluid. As in Ottavy et al. (2012), convective fluxes are discretized using an upwind third-order Roe scheme (Roe (1981)). The partial derivative equations are integrated with a cell-centered finite volume formulation method on a multi-block structured mesh, in the reference frame of each blade row. The system of equations is solved with the code *elsA*, which is jointly developed by ONERA and CERFACS (Cambier and Veuillot (2008)). Turbulence is modeled by the two-layer model k-ω Wilcox (Wilcox (1994)) and the flow is assumed to be fully turbulent as the Reynolds number based on the chord is around 10^6.

Dual time stepping is used to solve the unsteady flow, and the time marching for the inner loop is performed by using an implicit time integration scheme based on the backward Euler scheme and a scalar Lower-Upper Symmetric Successive Over-Relaxation (LU-SSOR) method (Yoon (1987)). The number of sub-iterations in the inner loop was chosen to ensure a reduction of two orders for the density residual magnitude.

Each rotation is discretized by 4,800 time steps, and the greatest mesh dimension in the circumferential direction is a little less than 1mm. According to the criterion proposed by Gourdain and Leboeuf (2009), the spatial and temporal discretization chosen can describe accurately frequencies up to about $2f_{BPF}$ with a third-order scheme of Roe. The aim is to simulate instabilities which have frequencies well below f_{BPF} so the discretization chosen is sufficient.

Meshing strategy and boundary conditions

The computational domain consists of the upstream test rig, the compressor and the downstream test rig (Fig.2a). For this configuration, the periodicity of the compressor and complete test rig is $2\pi/8$ up to the vertical exit of the rig, which is simulated as a 3D component. The domain was chosen this way as the final aim of this study is to simulate a surge cycle in the compressor and its complete test rig. Surge is a 1D, axial instability (Tauveron (2006)) therefore reducing the domain to $2\pi/8$ will not affect deeply the dynamics of surge. However it forces the number of stall cells to a multiple of 8.

Compressor part

The mesh consists of 27.5 million points for the $2\pi/8$ configuration. Each blade passage is divided into 7 domains, one O-grid around the blade and six H-grids for the rest of the domain. The rotors and the IGV have more points in the radial direction than stators because the tip gaps are meshed with 17 points radially. Stators are meshed with 310 000 grid points, rotors with 411 000 grid points. The IGV has 610 000 grid points because of its greater radial dimension. Since the simulation involves flow separation, a wall resolved mesh is used, and the size of the smallest cell in the normal direction is 10^{-6}m, which corresponds to y+ around 1. A sliding mesh condition with non-matching points is applied at rotor-stator interfaces. This method is conservative in the case of plane interfaces, which is the case here.

In order to check the quality of the mesh and numerical method chosen, a performance map has been drawn for a RANS simulation from choked massflow to near-surge operating points. This performance map has been compared to the results presented by Ottavy et al. (2012), which themselves had been compared finely to experimental results. They compare very well, which means that the numerical method and the grid predict the performance with an acceptable accuracy.

Test rig

The test rig was divided into four parts before meshing : the upstream settling chamber, the upstream strut, the downstream strut and the 3D exit. Both struts are meshed like stators. The settling chamber and the 3D exit were meshed separately. Since only low mach numbers occur in the test rig, the size of the mesh at walls in the normal direction is increased to 5.10^{-5}m. The upstream test rig has 6.6 million grid points, and the downstream test rig has 5.7 million grid points.

Boundary conditions

The choice of proper boundary conditions is of importance for the simulation of rotating stall. At near-surge conditions, the compressor map becomes flat, and a slight variation of pressure may result in a large variation of massflow. The pressure at the exit is not constant in time and the use of a fixed exit pressure may make convergence hard to obtain. This kind of boundary condition, called *stiff* by Vahdati et al. (2008) is not suitable for this kind of study. Instead, Vahdati (2005) recommends the use of a two variable nozzle, to allow the transient of the static pressure and achieve convergence at operating points near the maximum of pressure. As a consequence, a two-variable nozzle condition is applied at the exit of the downstream test rig, which simulates an idealized throttle condition with a quadratic law applied to it : $P_{s_{out}} = P_0 + k \cdot Q^2(t)$ with $P_{s_{out}}$ the static pressure applied at the exit, P_0 the reference static pressure, k the relaxation coefficient and Q the massflow through the exit. At the inlet of the domain, *i.e.* at the inlet of the settling chamber, fixed atmospheric boundary conditions are imposed through total pressure, total enthalpy and direction of the flow.

Aim of the study

The first simulation consists of 3 rotations of the compressor at a near-surge operating point, with established rotating stall in the last stage, after a transient flow of 7 rotations. The second simulation, with the complete test rig, consists of 10 rotations of the compressor for a near-surge operating point at which rotating stall occurs (Fig.2b), after the end of a transient flow of about 30 rotations. The operating points simulated can be found in Fig.2c, they are located in the region where the compressor map becomes flat. This compressor map is an instantaneous map from chocked to near-stall conditions. The aim of the study is to assess and explain the differences that exist between the two stall simulations.

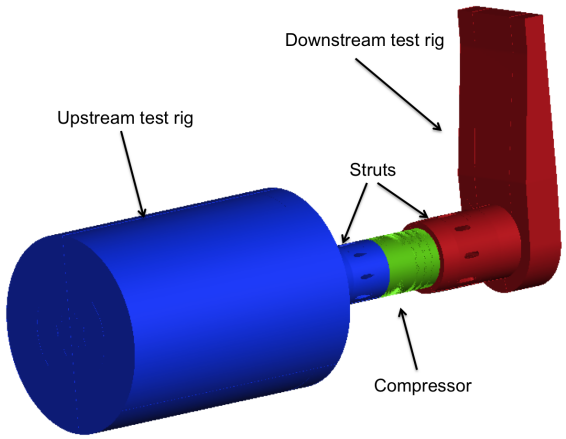

(a) 3D reconstitution of the simulated domain

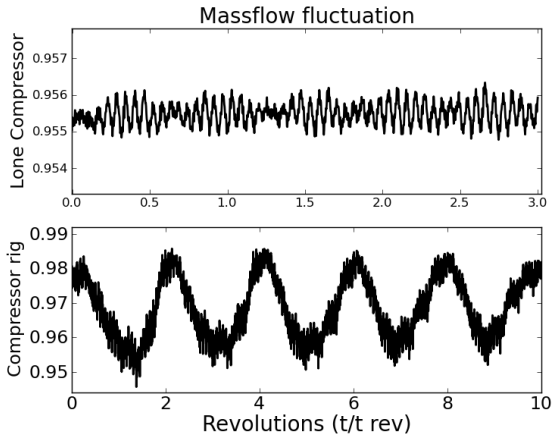

(b) Massflow time-histories

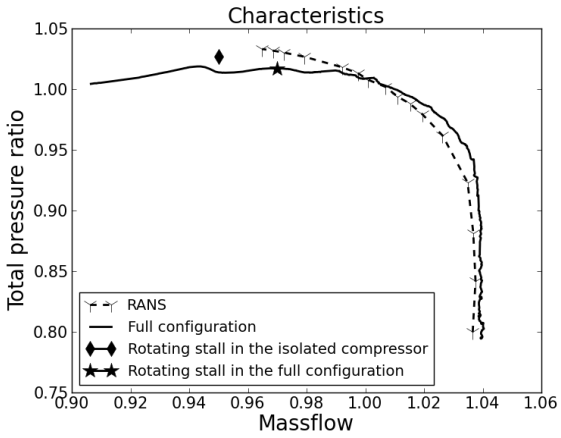

(c) Operating points simulated

Figure 2: Main characteristics of the two stall simulations

ANALYSIS OF NUMERICAL RESULTS

Theoretical tools

Tyler and Sofrin's model

In order to study RSI, Tyler and Tyler (1962) have proposed an analytical model to describe the pressure field in a compressor, showing the impact of blade-rows interactions on the flow. It predicts the spatio-temporal modes that develop in a compressor, resulting from the RSI. Given Ω, the rotating speed of the compressor, N_R and N_S respectively the number of rotor blades and stator blades, the wavelengths of the flow patterns that occur and their rotating speeds are given by the spatial mode m $(2\pi/\lambda)$:

$$m = aN_R + bN_S \quad \text{and} \quad \Omega_m = \frac{aN_R}{m}\Omega \tag{1}$$

with a,b relative integers.

The above model can easily be extended to an n-stage compressor and the spatial modes m and their rotation speeds are given by :

$$m = \sum_{i=1}^{n} (a_i N_{Ri} \pm b_i N_{Si}) \quad and \quad \Omega_m = \frac{\sum_{i=1}^{n} a_i N_{Ri}}{m}\Omega \tag{2}$$

This analysis shows that only rotors may create temporal modes, while stators may only create spatial modes. All the spatio-temporal modes due to RSI are given, however not all of them are observed in the simulation and on the contrary, some spatio-temporal modes not predicted by the model may occur. It is the case when a rotating structure appears, that does not have the same rotating speed as the shaft, such as rotating stall. When it occurs, the cells interact with the main flow, and they behave like a blade-row with given rotating speed and blade number, as suggested by Gourdain et al. (2010).

In the following paragraphs, spatial modes are expressed as a fraction of 2π (mode 24 means a wavelength of $2\pi/24$) and temporal modes are expressed as a multiple of the rotor frequency (mode 80 means the frequency is 80 times the rotor frequency). In the following paragraphs, spatio-temporal read n-m where n is the number of lobes around the annulus and m the temporal mode, *i.e.* non-dimensional frequency. The temporal modes can be converted to a frequency by multiplication by the shaft frequency 192.2Hz.

Cross-correlation in signal processing

Cross-correlation is a measure of similarity of two waveform signals, when a time-lag is applied to one of them. If f and g are two real functions, the cross correlation is a function of a time-lag and is defined as follow :

$$\begin{aligned} (f * g)(\tau) &= \int_{-\infty}^{+\infty} f(t)g(t-\tau)dt \quad \text{for continuous functions} \quad (a) \\ (f * g)(i) &= \sum_{i=-\infty}^{+\infty} f(n)g(n-i) \qquad \text{for discrete functions} \qquad (b) \end{aligned} \tag{3}$$

with *f(t)*, *g(t)* the temporal signals to analyze and τ, i the time lags applied to compute the cross-correlation.

Cross-correlation methods allow to analyze time signals and help determine the time delay, if it exists, between the two signals. The cross-correlation should be computed for every instant that the signals contain. A peak in the correlation function indicates that, by means of shifting one of the signals by the time delay at which the peak appears, the signals are aligned. An FFT (Fast Fourier Transform) can be applied to the correlation function. It shows the frequencies that correlates the two signals.

Spectral analysis applied to the isolated configuration

Part span stall appears for an average massflow of Q/Q_n=0.95 in CREATE. Figure 2b shows the evolution of the massflow downstream S3 during the 3 rotations simulated. The conservative variables were extracted in the test section 28A (see Fig.1b) upstream S3 at 83% of span, at a regular pace, in the fixed referential, during the whole simulation. Figure 3 shows a reconstitution of the full annulus by duplication colored by entropy. 24 zones in Fig.3a and 16 zones in Fig.3b exhibit a high level of entropy. They correspond to rotating stall cells.

The axial velocity at 83% of span was computed for all the circumferential grid points probed, which gives spatial and temporal data. First a spatial FFT is computed, which gives the spatial modes, then a temporal FFT is applied to each spatial mode, which gives the temporal modes associated to the spatial ones.

Figures 4a shows the amplitude of the spatial modes as a function of temporal modes. Among the expected modes, the spatio-temporal mode 80-80 can be found on the map. It is linked to R2 and R3 which both have 80 blades. The spatio-temporal mode 24-19 and three harmonics are of importance on the map. Temporal modes are given by a linear combination of even numbers in the case of CREATE, so the mode 24-19 could not be predicted by Tyler and Sofrin's model. The location and

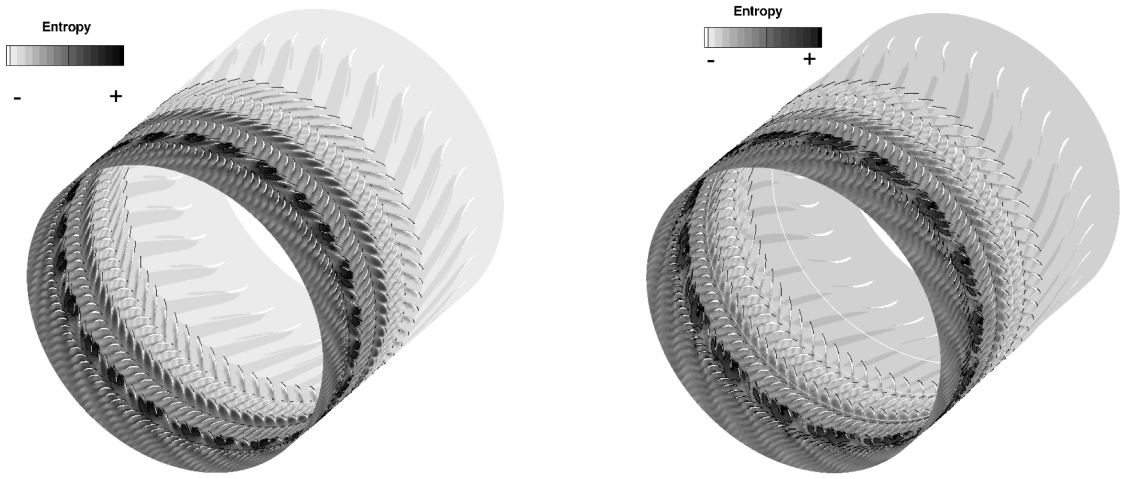

(a) Isolated compressor

(b) Compressor and complete test rig

Figure 3: Flow 83% span in plane 28A

the characteristics of the phenomenon indicates that rotating stall occurs in the last stage. It behaves like a rotor blade-row with 24 blades, rotating at a speed of: $\Omega_s = \frac{m_t}{n_{cell}}\Omega = \frac{19}{24}\Omega = 79\%$ of Ω.

Spectral analysis applied to the full configuration

For this configuration, a stable operating point with rotating stall was obtained for an averaged non-dimensional massflow of 0.97. Both low and high frequency oscillations modulate the massflow. As in the isolated configuration, conservative variables were probed at every rotor - stator interface at 83% of span, but also at 50% of span through the whole compressor and test rig. The modulation of the massflow through the compressor (Fig.2b) suggests that modified surge occurs. Modified surge is characterized by the simultaneous occurrence of a low frequency axial massflow oscillations and rotating stall. The following paragraphs show that rotating stall occurs and is local to the third stage, with a frequency of the order of 10^3Hz, whereas the low frequency is purely axial and affects the whole domain.

Rotating stall

One reference axial speed signal was chosen arbitrary at 83% of span of the R3-S3 interface (plane 28A Fig.1b), and a temporal cross-correlation function was computed with the probes of several other circumferential positions. An FFT was then applied to the correlation functions obtained. Fig.4c shows the frequencies contained in 2 signals at the same span in plane 28A, at two different circumferential positions. The amplitude of the frequency 2500 Hz (temporal mode 13 in Fig.4b) is the highest of all frequencies. Three harmonics also occur noticeably. The BPF's of the rotors (12 300Hz and 15 500 Hz, resp. temporal modes 64 and 80) are also visible but far weaker. Tyler and Sofrin's model cannot predict the temporal mode 13, which means that the rotating structure in the last stage of the compressor are rotating stall cells. A spatial FFT indicates that there are 16 cells (Fig.3b), the rotating speed of which is 81.25% of the shaft rotating speed (Fig.4b).

Low frequency oscillation

The low frequency oscillation that occurs in the compressor may be the low frequency component of modified surge only if it is an axial wave. This means that at any two different circumferential

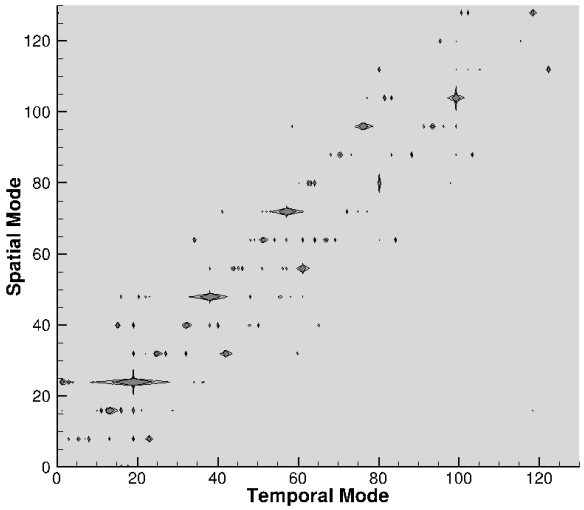

(a) Spatio-temporal modes at rotating stall in the isolated compressor

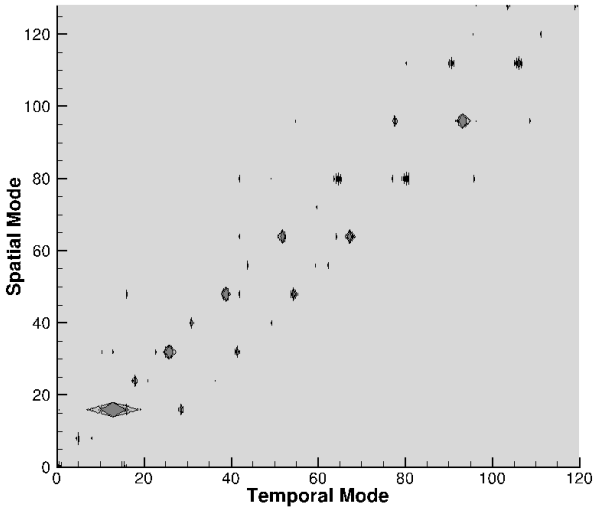

(b) Spatio-temporal modes at rotating stall in the compressor and test rig

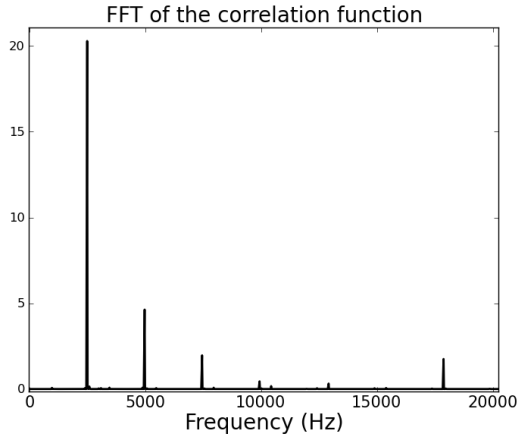

(c) FFT of the correlation function

Figure 4: Analysis of the probes at 83% of span on plane 28A

positions, the axial speeds probed must be in phase for that frequency, and that the low frequency must be found everywhere in the compressor.

Axial speed at 50% of span was probed at every rotor - stator interface. A temporal cross correlation function was computed between a signal in R1-S1 interface and one in R2-S2 interface, and between the signal in R1-S1 interface and the one in R3-S3 interface. In both cases, the frequency 94Hz appears and contains much energy. That result shows that this low frequency is found through the whole compressor. Figure 5c shows that the frequency 94Hz also affects upstream and downstream test rig parts, as this frequency corresponds to a period of about 2 rotations.

The frequency 2500Hz can also be seen but its relative importance is greatly reduced on Fig.5a and Fig.5b compared to its importance on Fig.4c, which shows that rotating stall is only local to the third stage.

Within the R3-S3 interface, at 83% of span, a cross correlation for a time-lag of 0 was computed between a signal at an arbitrary circumferential position and the signals of every other circumferential position. The cross-correlation was computed on low-pass filtered signals.That method aims at testing all the circumferential probes to see wether they are in phase for the low frequencies. The average and standard deviation of the correlation were also computed. The normalized average is equal to

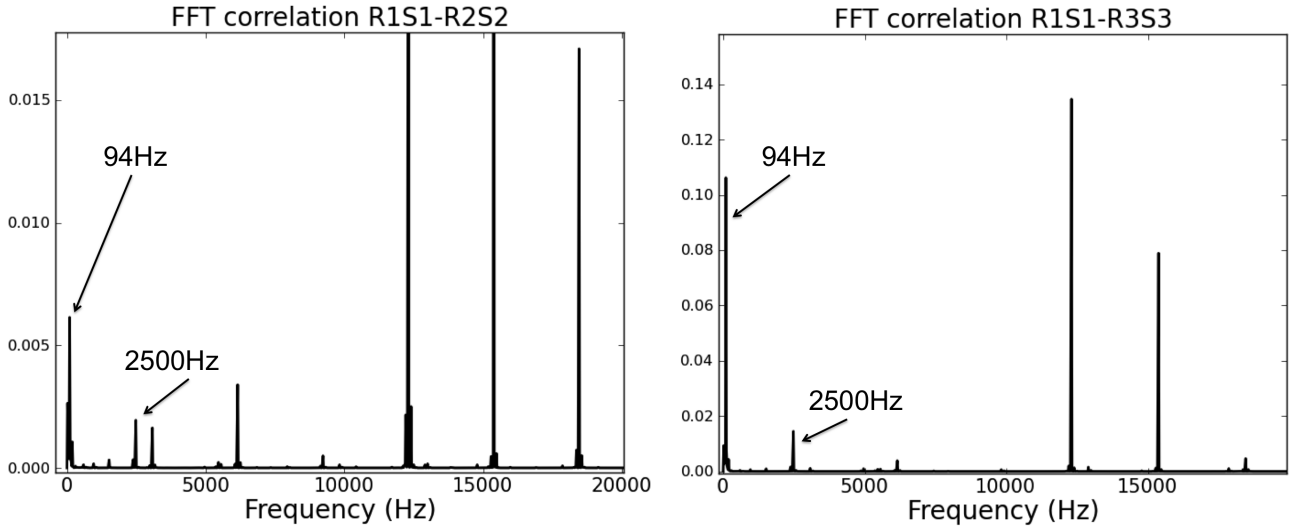

(a) FFT of the correlation function between R1-S1 and R2-S2 interfaces

(b) FFT of the correlation function between R1-S1 and R3-S3 interfaces

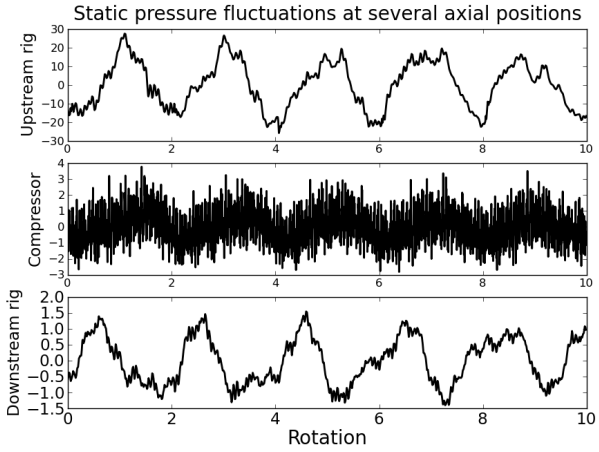

(c) Static pressure fluctuations through the whole configuration

Figure 5: Analysis of the low frequency oscillation

0.83 (i.e. close to 1) and the standard deviation is 0.073, which is low. That result indicates that all the circumferential probes oscillate in phase for the low frequencies, therefore the low frequencies in the flow are axial and the frequency 94Hz is a 1D axial wave.

As a conclusion, it has been proved that modified surge occurs in this configuration, as the low frequency oscillation is purely axial and has a frequency of 94Hz, and as rotating stall, which occurs in R3, has 16 cells and a frequency of 2500 Hz.

Comparison of the results

Major differences in the rotating stall flow patterns are caused by the addition of the experimental facility in the numerical simulation. They are summarized in Table 2.

Figure 4a and 4b indicate that the rotating stall mode in each configuration co-exists with the rotating stall mode of the other configuration, even though the latter contains far less energy. Indeed, the spatio-temporal mode 16-13 is visible in the isolated compressor (see Fig.4a) and the spatio-temporal mode 19-24 is also found in the compressor with the complete test rig (see Fig.4b). This confirms the results of the analytical models of Spakovszky (2001), Tauveron et al. (2006) and Greitzer and Moore

Table 2: Comparison of the patterns of rotating stall in the two simulations

Configuration	**Isolated**	**Full**
Mean massflow ($/Q_{ref}$)	0.95	0.97
Mean total pressure ratio ($/P_{ref}$)	1.027	1.017
Number of cells	24	16
Rotating speed of cells ($/\Omega$)	79,6%	81,25%
Phenomenon	Rotating stall	modified surge

(1985), which show the role of the entire system on the selection of the most unstable mode.

ACOUSTIC RESONANCE IN THE TEST RIG

The low frequency oscillation that affects static pressure can be seen all along the axial part of the test rig and compressor (Fig.5b). However, it is greatly reduced in the vertical exit of the downstream part of the test rig. The structure of the wave suggests an acoustic origin.

The in-house Helmholtz solver AVSP (Nicoud et al. (2007); Benoit (2004)) is a code dedicated to the computation of the thermo-acoustic modes in 3D configurations with no flow. However the code can be used assuming low Mach flow, perfect gas law, and low thermodiffusivity and viscosity (Poinsot and Veynante (2001)). AVSP is used here to compute the acoustic modes of the test rig and their amplitude. The computational domain is the same as the one used for the aerodynamic simulations (Fig.2a), however the full annulus is simulated and the blades have been removed as the hypothesis retained is that they interfere only slightly with low frequencies. The unstructured mesh consists of 65 000 tetrahedrons. The resonant frequencies computed by AVSP are given in Tab.3. The third mode (95.8Hz) is very close to the frequency found by elsA (94Hz).

Table 3: Resonant frequencies computed by AVSP

Mode number	**Mode 1**	**Mode 2**	**Mode 3**	**Mode 4**	**Mode 5**	**Mode 6**
Frequency	33.8Hz	40.2Hz	95.8Hz	110.6Hz	121.56Hz	121.60Hz

Fig 6a shows the streamwise evolution of the amplitude of the third mode computed by elsA and AVSP. Fig.6b gives an overview of the amplitude of the oscillation in the whole configuration computed by AVSP. The tendencies predicted by AVSP and elsA are the same : the amplitude is low in the test rig and becomes very high in the compressor. Three loops and two nodes of static pressure are found through the configuration and they are located almost at the same axial positions. The waves predicted by elsA and AVSP have the same frequency and a similar spatial structure, therefore the low frequency pressure oscillation found by elsA corresponds to the third acoustic mode of the compressor rig.

CONCLUSIONS

In this paper, the two numerical setups used to investigate rotating stall in the axial compressor CREATE are presented. The first configuration consists of CREATE alone, and the second one is the same compressor including the complete test rig. The results of the simulations at near-surge conditions are presented and analyzed using a modal approach and advanced signal processing methods. The study shows that the test rig induces major differences in the rotating stalls simulated, in terms of number of cells and their rotation speed. In the isolated configuration, the rotating stall has 24 cells and a rotating speed of 79% of Ω. In the full configuration, there are 16 cells and the rotation speed of the cells is 81.25% of Ω. Finally, the major difference between the two sets of results is the low frequency massflow oscillation which occurs in the full configuration, causing modified surge, whereas

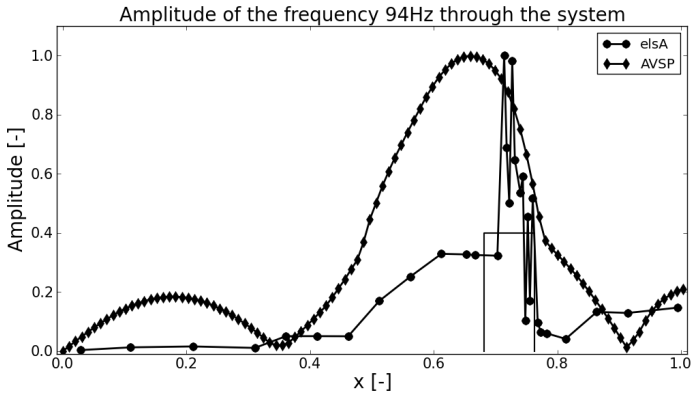

(a) Amplitude computed by elsA and AVSP

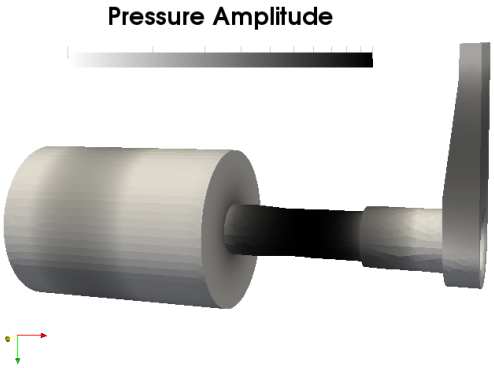

(b) Amplitude in the configuration (AVSP)

Figure 6: Amplitude of the pressure fluctuation due to the frequency 94Hz through the configuration

this phenomenon has not been found in the isolated compressor. The low frequency that characterizes modified surge in the full configuration is the third resonant mode of the configuration.

ACKNOWLEDGEMENTS

The authors wish to acknowledge the company Snecma (Safran group), the French DGAC and the CNRS, which supports the CREATE research program, and the company GENCI for their support on the calculator Curie on the project fac6074. The authors also wish to thank Francis Leboeuf, Florence De Crecy, Xavier Ottavy and Nicolas Courtiade from LMFA, and Thomas Leonard, Adrien Gomar, Francois Gallard, Ignacio Duran and Stephane Moreau from CERFACS for their help.

REFERENCES

D. Arnaud. *Analyse expérimentale des phénomènes instationnaires dans un compresseur multi-étages à forte charge aérodynamique*. PhD thesis, École Centrale de Lyon, 2003. Bonne intro aux phenomenes instationnaires dans les turbomachines (classification). These experimentale (mesure).

L. Benoit. Calculations of thermo-acoustic eigenmodes of an annular combustion chamber. Technical report, CERFACS , Lehrstuhl fur Thermodynamik, 2004.

S. Callot. *Analyse des Mecanismes Macroscopiques Produits par les Interactions Rotor/Stator dans les Turbomachines*. PhD thesis, Ecole Centrale de Lyon, 2002.

L. Cambier and J.P. Veuillot. Status of the elsA CFD Software for Flow Simulation and Multidisciplinary Applications. *46th AIAA Aerospace Science Meeting and Exhibit*, 2008.

A.J. Crook, E.M. Greitzer, C.S. Tan, and J.J. Adamczyk. Numerical Simulation of Compressor Endwall and Casing Treatment Flow Phenomena. *Journal Of Turbomachinery*, 115:501–512, 1993.

N. Gourdain and F. Leboeuf. Unsteady Simulation of an axial compressor stage with casing and blade passive treatment. *Journal of Turbomachinery@*, 131, 2009.

N. Gourdain, S. Burguburu, and F. Leboeuf. Rotating Stall Simulation and Analysis in axial Compressor. *ISABE*, page 10, 2005.

N. Gourdain, S. Burguburu, F. Leboeuf, and G. Michon. Simulation of rotating stall in a whole stage of an axial compressor. *Computer and Fluids*, 39:1644–1655, 2010.

Greitzer. Surge and Rotating stall in axial flow compressor, Part I : Theoretical Compression System Model, Part II : Experimental Results and Comparison with Theory. *Transaction of the ASME*, 98: 190–217, 1976.

E.M. Greitzer and F.K Moore. A theory of post-stall transients in axial compression systems: part I Development of equations, part II Applications. *ASME*, 1985.

D.A. Hoying. *Blade Passage Flow Structure Effects on Axial Compressor Rotating Stall Inception*. PhD thesis, Massachusetts Institute of Technology, 1996.

M. Inoue, M. Kuroumaru, S. Yoshida, T. Minami, K. Yamada, and M. Furukawa. Effect of Tip Clearance on Stall Evolution Process in a Low-Speed Axial Compressor Stage. *ASME Turbo Expo*, paper GT2004- 53354, 2004.

F. Nicoud, L. Benoit, C. Sensiau, and T. Poinsot. Acoustic modes in combustors with complex impedances and multidimensional active flames. *AIAA Journal*, 45:426–441, 2007.

X. Ottavy, N. Courtiade, and Gourdain N. Experimental and Computational Methods for Flow Investigation in High-Speed Multistage Compressor. *Journal Of Propulsion and Power*, 28:1141–1155, 2012.

T. Poinsot and D. Veynante. Theoretical and numerical combustion - First Edition. , page 473, 2001.

P. L. Roe. Approximate Riemann Solvers, Parameter Vectors and Difference Schemes. *Journal of Computational Physics*, 43, 1981. pp. 357-372.

Z. Spakovszky. *Application of Axial and Radial Compressor Dynamic System Modeling*. PhD thesis, Massachusetts Institute of Technology, 2001.

N. Tauveron. Simulation of surge inception and performance of axial multistage compressor. *Proceedings of ASME Turbo Expo 2006*, 2006.

N. Tauveron, P. Ferrand, F. Leboeuf, N. Gourdain, and S. Burguburu. A numerical contribution to the analysis of surge inception and development in axial compressors. *ISUAAAT conference*, 2006.

T. Tyler, J. & Sofrin. Axial Flow Compressor Noise Studies. *SAE Transactions*, 70:309–332, 1962.

M. Vahdati. On the Use of Atmospheric Boundary Conditions for Axial-Flow Compressor Stall Simulations. *Journal of Turbomachinery*, 127(3):349–351, 2005.

M. Vahdati, G. Simpson, and M. Imregun. Unsteady Flow and Aeroelasticity Behavior of Aeroengine Core-compressor rotating stall simulation with a multi-bladerow model. *Journal of Turbomachinery - Transactions of the ASME*, 130, 2008.

C. Wilcox, D. *Turbulence Modeling for CFD*. DCW Industries, Inc., La Cañada, CA, 2nd edition, 1994.

A. Yoon, S. Jameson. An LU-SSOR Scheme for the Euler and Navier-Stokes Equations. In *AIAA 25th Aerospace Sciences Meeting*, number AIAA-87-0600, Reno, Nevada, USA, january 12-15 1987.